Journal of Ceramic Processing Research. Vol. 17, No. 6, pp. 606~610 (2016)

J O U R N A L O F
Ceramic Processing Research

Simultaneously synthesis and sintering of a nanostructured Ti-Al_2O_3 composite by pulsed current activated heating

Jin-Kook Yoon[a] and In-Jin Shon[b,*]

[a]*Materials Architecturing Research Center, Korea Institute of Science and Technology, PO Box 131, Cheongryang, Seoul 130 650, Korea*

[b]*Division of Advanced Materials Engineering, the Research Center of Hydrogen Fuel Cell, Chonbuk National University, 664-14 Deokjin-dong 1-ga, Deokjin-gu, Jeonju, Jeonbuk 561-756, Korea*

Nanopowders of TiO and Al were fabricated using high energy ball milling. Dense nanostuctured 3Ti-Al_2O_3 composite was simultaneously synthesized and sintered by pulsed current activated heating within 2 min in one step from mechanically activated powders of 3TiO and 2Al. The advantage of this process is that it allows very quick densification to near theoretical density and prohibition of grain growth in nanostructured materials. Highly dense 3Ti-Al_2O_3 with relative density of up to 99.9% was produced under simultaneous application of a 80 MPa pressure and the pulsed current. The average hardness and fracture toughness values of the composite were 1439 kg/mm^2 and 7 MPa · m$^{1/2}$, respectively.

Key words: Synthesis, Composite materials, Nanomaterials, Mechanical properties, Sintering.

Introduction

The most commonly used bearing couple in prosthetic hip or knee joint replacements consist of a cobalt-chrome (CoCr) metal alloy articulating against ultrahigh-molecular-weight polyethylene [1]. However, the CoCr metal alloy generates wear debris in prosthetic hip and knee bearing due to its low hardness. These wear debris have a negative role in producing tissue inflammation adjacent to the bearing. Therefore, alumina and zirconia ceramics have been used as alternatives to cobalt-chrome (CoCr) in total hip arthroplasty and total knee arthroplasty since the 1970s [2-6]. However, even though ceramic materials having high hardness reduces wear debris materials, they cannot satisfy the properties of prosthetic hip or knee join replacements because of its low resistance to the propagation of cracks. The brittle behavior of ceramics is manifested in their low fracture toughness values, which are lower than those of the metals used in orthopedic surgery. Thus, bearing materials in prosthetic hip or knee joint replacements basically require high hardness and high fracture toughness.

To cope with this problem, we fabricated a nanostructured metal-ceramic composite adding Ti to improve the fracture toughness of Al_2O_3. Ti has a density of 4.54 g · cm^{-3}, a Young's modulus of 116 GPa and good fracture toughness and biocompatibility. In addition, as titanium and alumina have a similar coefficient of thermal expansion, these cermets will have a better performance than other materials [7]. Therefore, the metal matrix composites are recognized as candidates for aerospace, automotive, bio-materials and defense applications. Traditionally, discontinuously reinforced metal matrix composites have been produced by several processing routes such as powder metallurgy, spray deposition, mechanical alloying, various casting techniques and SHS(self-propagating high temperature synthesis). One of all these techniques, high energy ball milling and mechanical alloying of powder mixtures, were reported to be efficient techniques for the preparation of nano-crystalline metals and alloys, which is a combination of mechanical milling and chemical reactions [8, 9]. Nanocrystalline materials have received much attention as advanced engineering materials with improved physical and mechanical properties [10-12]. In recent days, nanocrystalline powders have been developed by the thermochemical and thermomechanical process named as the spray conversion process (SCP), co-precipitation and high energy milling [13-15]. However, the grain size in sintered materials becomes much larger than that in pre-sintered powders due to a fast grain growth during conventional sintering process. So, controlling grain growth during sintering is one of the keys to the commercial success of nanostructured materials. In this regard, the pulsed current activated sintering method which can make dense materials within 2 min, has been shown to be effective in achieving this goal [16-18].

The purpose of this work is to produce dense nanocrystalline 3Ti-Al_2O_3 composite within 2 min in

*Corresponding author:
Tel : +82-63-270-2381
Fax: +82-63-270-2386
E-mail: ijshon@chonbuk.ac.kr

one-step from mixtures of mechanically activated 3TiO and 2Al powders by using this pulsed current activated sintering method and to evaluate its mechanical properties and grain size.

Experimental Procedures

Powders of 99.5% TiO (< 5 μm mesh, Alfa company) and 99.5% pure Al (–325 mesh, Alfa company) were used as a starting materials. $3TiO_2$ and 2Al powder mixtures were first milled in a high-energy ball mill, Pulverisette-5 planetary mill with 250 rpm and for 10 hrs. Tungsten carbide balls (10 mm in diameter) were used in a sealed cylindrical stainless steel vial under argon atmosphere. The weight ratio of ball-to-powder was 20 : 1. The grain size of the powders was calculated from the full width at half-maximum (FWHM) of the diffraction peak by Suryanarayana and Grant Norton's formula [19].

$$B_r(B_{crystalline} + B_{strain}) \cos\theta = k\,\lambda / L + \eta\sin\theta \quad (1)$$

where B_r is the full width at half-maximum (FWHM) of the diffraction peak after instrumental correction; $B_{crystalline}$ and B_{strain} are FWHM caused by small grain size and internal stress, respectively; k is constant (with a value of 0.9); λ is wavelength of the X-ray radiation; L and η are grain size and internal strain, respectively; and θ is the Bragg angle. The parameters B and B_r follow Cauchy's form with the relationship: $B = B_r + B_s$, where B and B_s are the FWHM of the broadened Bragg peaks and the standard sample's Bragg peaks, respectively.

The milled powders were placed in a graphite die (outside diameter, 35 mm; inside diameter, 10 mm; height, 40 mm) and then introduced into the pulsed current activated sintering (PCAS) system made by Eltek Co. in the Republic of Korea. A schematic diagram of this system is shown in Fig. 1. The PCAS apparatus includes a 30 kW power supply and a uniaxial press with a maximum load of 50 kN. The system was first evacuated and a uniaxial pressure of 80 MPa was applied. A pulsed current (on time; 20 μs, off time; 10 μs) was then activated and maintained until the densification rate became negligible, as indicated by the observed shrinkage of the sample. Sample shrinkage was measured in real time by a linear gauge measuring the vertical displacement. Temperature was measured by a pyrometer focused on the surface of the graphite die. A temperature gradient from the surface to the center of the sample is dependent on the heating rate, the electrical and thermal conductivities of the compact, and its relative density. The heating rates were approximately 1000 K $minute^{-1}$ during the process. At the end of the process, the current was turned off and the sample was allowed to cool to room temperature. The entire process of densification using the PCAS technique consists of four major control stages: chamber evacuation, pressure application, power application, and cooling off. The process was carried out under a vacuum of 5.33 Pa.

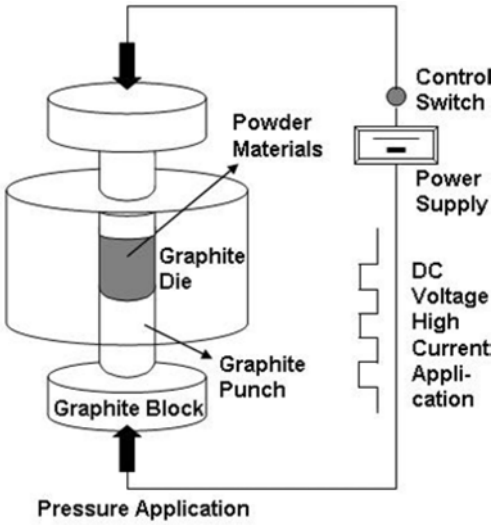

Fig. 1. Schematic diagram of the apparatus for pulsed current activated sintering.

The relative densities of the sintered samples were measured by the Archimedes method. Microstructural information was obtained from the fracture surfaces. Compositional and microstructural analyses of the samples were carried out through X-ray diffraction (XRD), and field-emission scanning electron microscopy (FE-SEM). Vickers hardness was measured by performing indentations at a load of 20 kg_f with a dwell time of 15 s.

Results and Discussion

The interaction between 3TiO and 2Al, i.e.,

$$3TiO + 2Al \rightarrow 3Ti + Al_2O_3 \quad (2)$$

is thermodynamically feasible as shown in Fig. 2. XRD patterns of raw materials and milled powder is shown in Fig. 3. In Fig. 3(c), reactant TiO and Al peaks were detected and product peaks of Ti and Al_2O_3 were not observed. From the results, synthesis does not occur during the high energy ball milling. The full width at half-maximum of the diffraction peak in milled powder is wider than that of raw powder due to strain and refinement of grain size. Fig. 4 shows plot of $B_r\cos\theta$ versus $\sin\theta$ for TiO and Al. The average grain sizes of TiO and Al measured by Suryanarayana and Grant Norton's formula [19] were about 15 nm and 35 nm, respectively. FE-SEM image and EDS analysis of 3TiO and 2Al powders milled by high energy ball milling method for 10 h are shown in Fig. 5. The powders are very fine and have a some agglomeration. The milling process is known to introduce impurities from the ball and/or container. However, in this study, peaks other than Ti, Al and O were not identified.

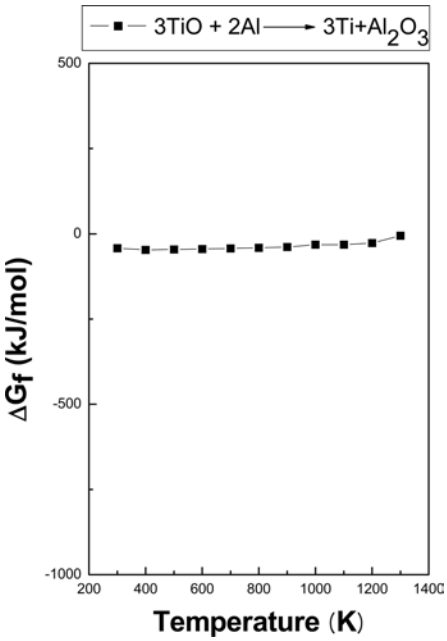

Fig. 2. Temperature dependence of the Gibbs free energy change for the interaction between titanium oxide and aluminium.

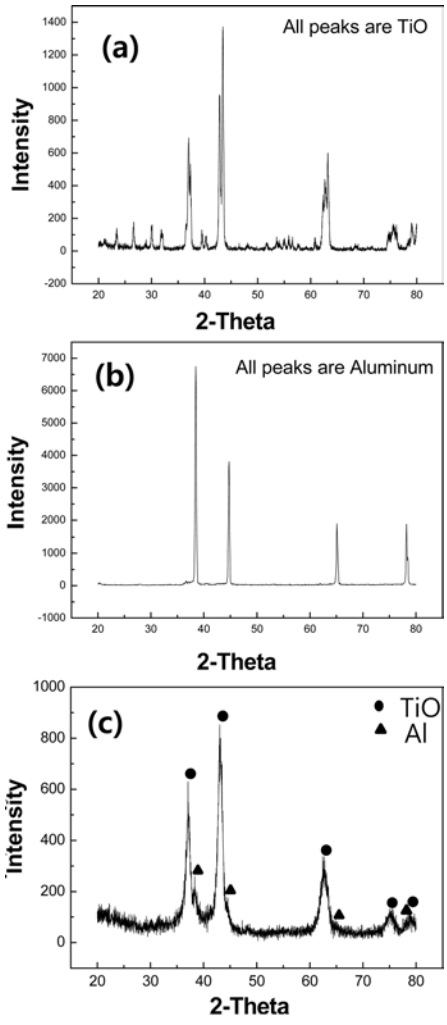

Fig. 3. XRD patterns of raw materials and mechanically milled powder: (a) TiO, (b) Al and (c) mechanically milled 3TiO-2Al.

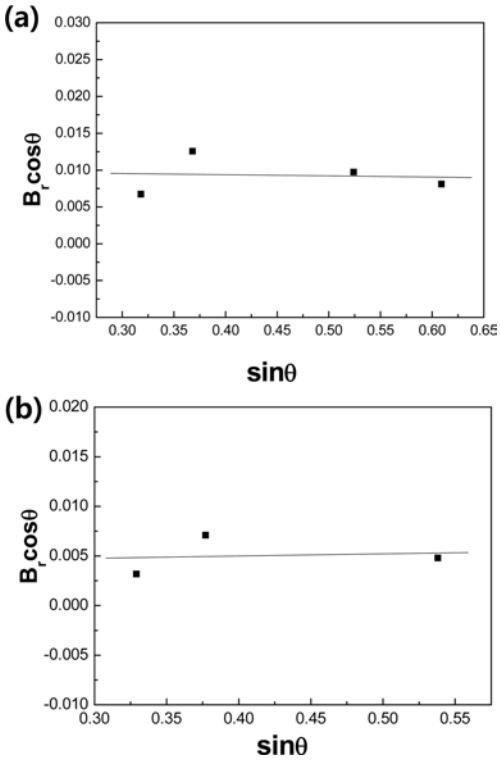

Fig. 4. Plot of $B_r$cosè versus sinè for (a) TiO and (b) Al milled for 10 h.

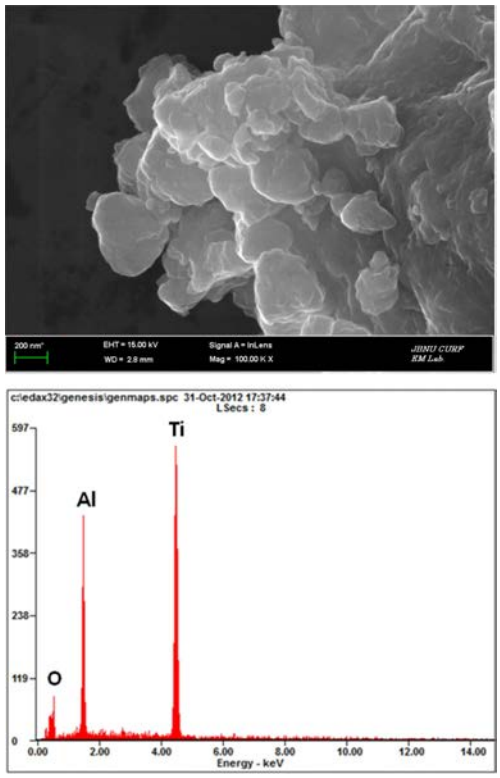

Fig. 5. FE-SEM image and EDS analysis of the 3 TiO and Al powders milled for 10 h.

Fig. 6 shows the variations in shrinkage displacement and temperature of the surface of the graphite die with heating time during the processing of 3TiO and 2Al system. As the pulsed current was applied the specimen

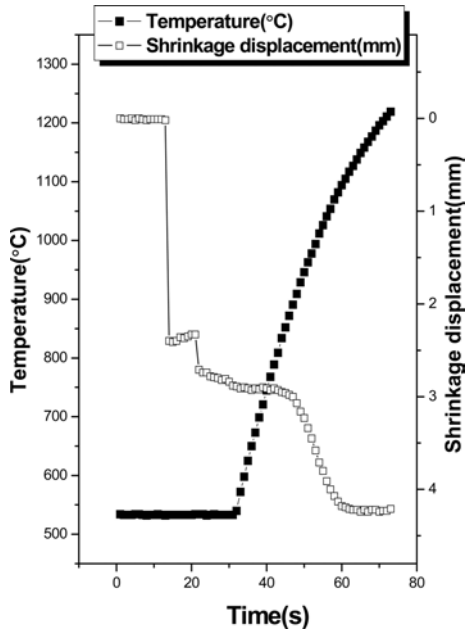

Fig. 6. Variations of temperature and shrinkage displacement with heating time during high frequency induction heated combustion of 3TiO-2Al system.

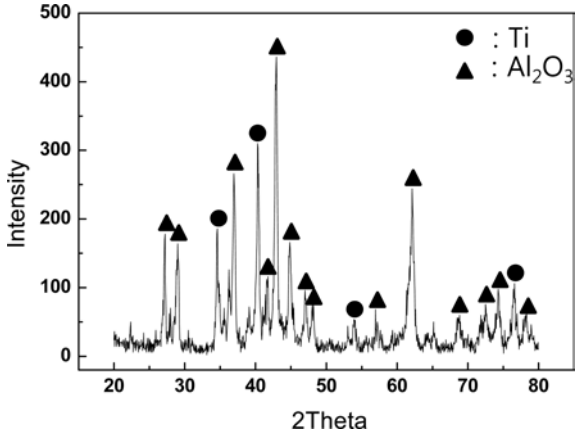

Fig. 7. XRD pattern of the 3Ti-Al_2O_3 composite sintered by PCAS.

showed the shrinkage displacement was nearly constant up to heating time of 10 s but then abruptly increased. And the shrinkage displacement gradually increased with temperature up to about 1220 °C. Fig. 7 shows X-ray diffraction result of a specimen heated to 1220 °C. The figure exhibit only peaks pertaining to the Ti and Al_2O_3. From the result, simultaneous synthesis and densification occurs during the heating under the 80 MPa pressure. FE-SEM image of an etched surface of the samples heated to 1220 °C under a pressure of 80 MPa is shown in Fig. 8. A complete reaction between these elements (3TiO and 2Al) has taken place under these conditions. These conclusions were supported by X-ray diffraction analyses with peaks of the product phase (Ti and Al_2O_3 phase). The microstructure consists of nanophases. The corresponding relative density is about 99.9%. The

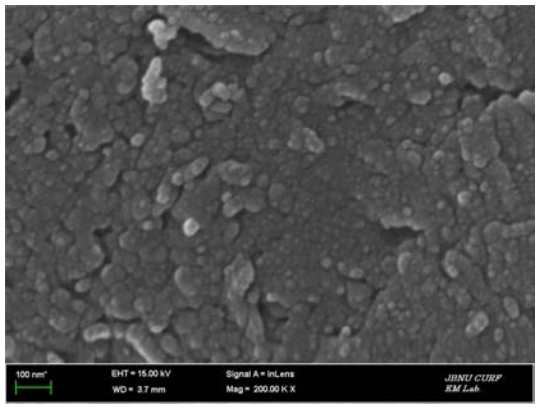

Fig. 8. FE-SEM of the 3Ti-Al_2O_3 composite sintered by PCAS.

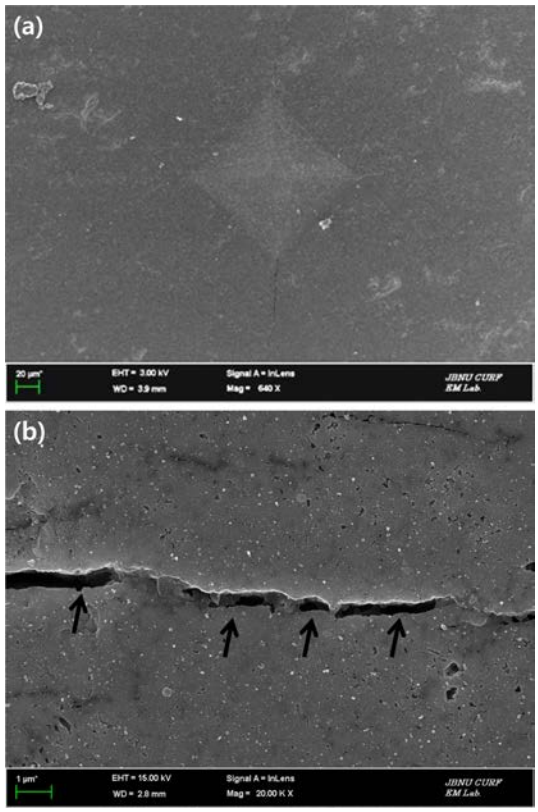

Fig. 9. Vickers hardness indentation and crack propagation in 3Ti-Al_2O_3 composite produced by PCAS.

structure parameters, i.e. the average grain sizes of Ti and Al_2O_3 are obtained from by Suryanarayana and Grant Norton's formula [19], were 80 nm and 50 nm, respectively. The abrupt increase in the shrinkage displacement at the ignition temperature is due to the increase in density as a result of molar volume change associated with the formation of Ti and Al_2O_3 from 3TiO and 2Al reactant and the consolidation of the product.

Vickers hardness measurements were made on polished sections of the 3Ti-Al_2O_3 composite using a 20 kg_f load and 15 s dwell time. The calculated hardness value of 3Ti-Al_2O_3 composite was 1439 kg/mm^2. This value represents

an average of five measurements. The length of these cracks permits an estimation of the fracture toughness of the material. From the length of these cracks, fracture toughness values can be determined using two expressions. The expression, proposed by Anstis et al. [20] is

$$K_{IC} = 0.016\ (E/H)^{1/2} \cdot P/C^{3/2} \quad (3)$$

where E is Young's modulus, H the indentation hardness, P the indentation load, and C the trace length of the crack measured from the center of the indentation. The modulus was estimated by the rule mixtures for the 0.45 volume fraction of Al_2O_3 and the 0.55 volume fraction of Ti using $E(Al_2O_3) = 336$ GPa [21] and $E(Ti) = 116$ GPa [22].

As in the case of hardness values, the toughness values were derived from the average of five measurements. The toughness value obtained by the method of calculation was 7 MPa · $m^{1/2}$. The hardness and fracture toughness of Al_2O_3 with grain size of 4.5 μm are reported as 1800 kg/mm^2 and 4 MPa · $m^{1/2}$, respectively [1]. The hardness of 3Ti-Al_2O_3 composite is lower than that of monolithic Al_2O_3 but the fracture toughness is higher than the value of Al_2O_3 due to addition of ductile Ti. Fig. Fig 9 shows Vickers hardness indentations and a crack propagation in the 3Ti-Al_2O_3 composite. Cracks were radially propagated from the indentation as shown in Fig. 9(a). Fig. 9(b) shows a crack propagated in a deflective manner (↑) in 3Ti-Al_2O_3 composite. The enhanced fracture toughness of 3Ti-Al_2O_3 composite is believed that Ti and Al_2O_3 in the composite may deter the propagation of cracks and Ti and Al_2O_3 have nanostructure phases.

Conclusions

Using the pulsed current activated sintering method, the simultaneous synthesis and densification of nanostructured 3Ti-Al_2O_3 composite was accomplished from mechanically activated powders of 3TiO and 2Al. Complete synthesis and densification can be achieved in one step within duration of 2 min. The relative density of the composite was 99.9 % for the applied pressure of 80 MPa and the pulsed current. The average grain sizes of Ti and Al_2O_3 prepared by pulsed current activated sintering were about 80 nm and 50 nm, respectively. The average hardness and fracture toughness values obtained were 1439 kg/mm^2 and 7 MPa · $m^{1/2}$, respectively.

Acknowledgments

This work was supported by the KIST Institutional Program (Project No. 2E25374-15-096) and this work was supported by the Korea Institute of Energy Technology Evaluation and Planning (KETEP) and the Ministry of Trade, Industry & Energy(MOTIE) of the Republic of Korea (No. 20164030201070) and this research was supported by Basic Science Research Program though the National Research Foundation of Korea (NRF) funded by the Ministry of Education (2015R1D1A1A01056600).

References

1. M.N. Rahaman, A. Yao, B.S. Bal, J.P. Garino, and M.D. Ries, J. Am. Ceram. Soc. 90 (2007) 1965-1988.
2. D. Hannouche, M. Hamadouche, and R. Nizard, Clin. Orthop. Relat. Res. 430 (2005) 62-71.
3. R. Nizard, L. Sedel, and D. Hannouche, J. Bone Joint Surg. Br. 87 (2005) 755-758.
4. L. Sedel, R. Nizard, and P. Bizot, Semin. Arthroplasty 9 (1998) 123-134.
5. M. Akagi, T. Nakamura, Y. Matsusue, T. Ueo, K. Nishijyo, and E. Ohnishi J. Bone Joint Surg. Am. 82-A (2000) 1626-1633.
6. H. Oonishi, M. Aono, and N. Murata, Clin. Orthop. Relat. Res. 282 (1992) 95-104.
7. G.P. Kelkar, and A.H. Carim, J. Am. Ceram. Soc. 78 (1995) 572-576.
8. H.G. Jo and I.J. Shon, Journal of Ceramic Processing Research 15[6] (2014) 371-375.
9. I.J. Shon, Korean J. Met. Mater. 52 (2014) 573-580.
10. In-Jin Shon, Hyoung-Gon Jo, Byung-Su Kim, Jin-Kook Yoon, and Kyung-Tae Hong, Korean J. Met. Mater., 53 (2015) 474-479.
11. H. S. Kang, J. M. Doh, J. K. Yoon, and I. J. Shon, Korean J. Met. Mater., vol. 52, no. 10 (2014) 777-782.
12. So-Mang Kwon, Na-Ra Park, Jae-Won Shin, Se-Hoon Oh, Byung-Su Kim, and In-Jin Shon, Korean J. Met. Mater., 53 (2015) 555-562.
13. Z. Fang, and J.W. Eason JW, Int. J. Refract. Met. Hard Mater. 13 (1995) 297-303.
14. A.I.Y. Tok, L.H. Luo, F.Y.C. Boey, Mater. Sci. Eng. A 383 (2004) 229-234.
15. Bo-Ram Kang, Jin-kook Yoon, Kyung-Tae Hong, and In-Jin Shon, Met. Mater. Int., 21[4] (2015) 698-703.
16. I.J. Shon, H.S. Kang, J.M. Doh, and J.K. Yoon, Met. Mater. Int., 21[2] (2015) 345-349.
17. Bo-Ram Kang and In-Jin Shon, Korean J. Met. Mater., 53 (2015) 320-325.
18. I.J. Shon, H.G. Jo, and H.J. Kwon, Korean J. Met. Mater. 52 (2014) 343-346.
19. C.Suryanarayana, and M. Grant Norton, X-ray Diffraction A Practical Approach, Plenum Press, New York, (1998).
20. G.R. Anstis, P. Chantikul, B.R. Lawn, and D.B. Marshall, J. Am. Ceram. Soc. 64 (1981) 533-538.
21. W.G. Fahrenholtz, D.T. Ellerby and R.E. Loehman, J. Am. Ceram. Soc. 83 (2000) 1279-1280.
22. http://en.wikipedia.org/wiki/Elastic properties of the elements (data page).